

**Structures and stability of novel transition-metal ( $M = \text{Co, Rh, and Ir}$ ) borides**Yachun Wang,<sup>1</sup> Lailei Wu,<sup>1</sup> Yangzheng Lin,<sup>2</sup> Qingyang Hu,<sup>2,3</sup> Zhiping Li,<sup>4</sup> Hanyu Liu,<sup>5</sup> Yunkun Zhang,<sup>1</sup> Huiyang Gou,<sup>2,3,\*</sup> Yansun Yao,<sup>5,6,†</sup> Jingwu Zhang,<sup>1</sup> Faming Gao,<sup>4</sup> and Ho-kwang Mao<sup>2,3</sup><sup>1</sup>*Key Laboratory of Metastable Materials Science and Technology, College of Material Science and Engineering, Yanshan University, Qinhuangdao 066004, People's Republic of China*<sup>2</sup>*Geophysical Laboratory, Carnegie Institution of Washington, 5251 Broad Branch Road NW, Washington, D.C. 20015, USA*<sup>3</sup>*Center for High Pressure Science and Technology Advanced Research, Shanghai 201203, People's Republic of China*<sup>4</sup>*Key Laboratory of Applied Chemistry, College of Environmental and Chemical Engineering, Yanshan University, Qinhuangdao 066004, People's Republic of China*<sup>5</sup>*Department of Physics and Engineering Physics, University of Saskatchewan, Saskatoon, Canada, S7N 5E2*<sup>6</sup>*Canadian Light Source, Saskatoon, Canada, S7N 2V3*

(Received 4 August 2015; revised manuscript received 17 September 2015; published 9 November 2015)

Recent progress of high-pressure technology enables the synthesis of novel metal borides with diverse compositions and interesting properties. A precise characterization of these borides, however, is sometimes hindered by multiphase intergrowth and grain-size limitation in the synthesis process. Here, we theoretically explored new transition-metal borides ( $M = \text{Co, Rh, and Ir}$ ) using a global structure searching method and discovered a series of stable compounds in this family. The predicted phases display a rich variety of stoichiometries and distinct boron networks resulting from the electron-deficient environments. Significantly, we identified a new  $\text{IrB}_{1.25}$  structure as the long-sought structure of the first synthesized Ir-B compound. The simulated x-ray diffraction pattern of the proposed  $\text{IrB}_{1.25}$  structure matches well with the experiment, and the convex hull calculation establishes its thermodynamic stability. Results of the present paper should advance the understanding of transition-metal borides and stimulate experimental explorations of these new and promising materials.

DOI: [10.1103/PhysRevB.92.174106](https://doi.org/10.1103/PhysRevB.92.174106)

PACS number(s): 81.05.Zx, 61.66.Fn, 61.50.Ks, 71.15.Mb

**I. INTRODUCTION**

Transition-metal borides have attracted considerable investigations in recent years for their outstanding properties and growing applications in industry [1–11]. A unique electron-deficient bonding environment, as seen in many materials containing boron, enables a rich diversity of stoichiometries and structures of borides. In transition-metal borides, boron can form different polyhedral structures, ranging from symmetric clusters to extended networks, and exhibit fascinating properties, such as superconductivity [12,13], superhardness [14,15], and topological properties [16–19]. Recent progress in this field includes the identification of two hard borides,  $\text{CrB}_4$  and  $\text{MnB}_4$ , using single-crystal diffraction techniques and density functional calculations [20–22], and the synthesis of superconducting  $\text{FeB}_4$  under high-pressure conditions [23]. These studies advanced the understanding of transition-metal borides and led to an increasing interest in search for new members in this family [24–26].

Binary borides containing group 9 metals (Co, Rh, and Ir) have been extensively studied as catalysts and resistant coatings [27–32]. The emphasis of past studies has been primarily on the metal-rich borides. The boron-rich borides of this group are relatively less explored; up to now, there have only been two known phases. The first phase was an Ir-B compound synthesized in 1962 with an unidentified

crystal structure [33]. The composition of this compound was initially suggested as  $\text{IrB}_{1.5}$ , but other studies indicated that  $\text{IrB}_{1.35}$  or  $\text{IrB}_{1.25}$  were both possible [34,35]. In 2009, the same Ir-B compound was successfully fabricated in thin films that exhibited outstanding superhard behaviors [36]. The structure and stoichiometry of this Ir-B compound has not been solved, which partially motivated the present paper. In 2014, the second member to this family,  $\text{CoB}_{3.2}$  ( $\text{Co}_5\text{B}_{16}$ ), was successfully synthesized under high-pressure high-temperature conditions [30].

Theoretical studies have often been employed to identify new materials prior to their realizations. Recent advances of the theoretical tools, in particular, made it possible to systematically investigate the phase diagrams of unknown compounds. In the present paper, we performed a theoretical investigation of group 9 metal borides, with the emphasis on the boron-rich side. The structure searches were carried out using the particle swarm optimization (PSO) algorithm [37,38] combined with density functional optimizations. We have addressed the long-standing question on the composition and structure of the first Ir-B compound; the predicted structure model can well reproduce the experimental diffraction patterns, which is a significant step toward the identification of this material. In addition, the present paper discusses a series of new crystalline  $\text{MB}_x$  phases ( $M = \text{Co, Rh, and Ir}$ ;  $x = 1.5, 2, 3, 4,$  and  $6$ ) that are stable at ambient or high pressures or both. By changing the chemical compositions, one is able to manipulate the bonding pattern of the boron framework that dictates the mechanic and electronic properties of the system. Such information is of great importance to the understanding of metal-boron interactions in solids.

\*Author to whom correspondence should be addressed: [Huiyang.gou@gmail.com](mailto:Huiyang.gou@gmail.com)†[yansun.yao@usask.ca](mailto:yansun.yao@usask.ca)

## II. METHODS

Global structural searches were performed using the crystal structure analysis by particle swarm optimization (CALYPSO) code with a variable cell PSO algorithm [37,38], which has been successfully applied for tungsten and lithium borides [39,40]. Simulation cells containing up to 6 f.u. of cobalt, rhodium, and iridium borides ( $MB_x$ ,  $x = 1.5, 2, 3, 4$ , and 6) are studied for their stability at 1 bar and 50 and 100 GPa. Furthermore, crystal structures of the compounds that are chemically similar to  $MB_x$  were also considered as the candidate structures of  $MB_x$ . Candidate structures of  $MB_x$  obtained in the structure searches were fully optimized within the framework of density functional theory (DFT) as implemented in the Cambridge Serial Total Energy Package (CASTEP) software package [41]. The exchange and correlation of the electrons were treated by the generalized gradient approximation with Perdew-Burke-Ernzerhof (GGA-PBE) functional [42]. A cutoff energy of 400 eV and a dense  $k$ -point mesh [43] with spacing of  $0.3 \text{ \AA}^{-1}$  were employed. Phonon calculations were carried out by using finite displacement methods as implemented in the phonopy code [44]. Enthalpy of formation ( $\Delta H_f$ ) of borides was calculated as

$$\Delta H_f = H(MB_x) - H(M) - xH(B), \quad (1)$$

for decomposition products of  $M$  and  $B$  solids or

$$\Delta H_f = H(MB_x) - H(MB) - (x - 1)H(B), \quad (2)$$

for decomposition products of  $MB$  and  $B$  solids. Here,  $H(MB_x)$  is the enthalpy of  $MB_x$ , whereas  $H(M)$ ,  $H(MB)$ , and  $H(B)$  are the enthalpies of referential phases of  $M$ ,  $MB$ , and  $B$  under the given pressure. The hexagonal phase of Co, cubic phase of Rh and Ir were taken as the referential phases of metals, respectively. The  $\alpha$ -B and  $\gamma$ -B (for high-pressure calculations above 20 GPa [45]) were employed as the referential phases of B.

## III. RESULTS AND DISCUSSION

The structural searches started with the  $M_2B_3$  (or  $MB_{1.5}$ ) stoichiometry that was initially suggested for the Ir-B system. At ambient pressure, the ground state structures of  $Ir_2B_3$ ,  $Rh_2B_3$ , and  $Co_2B_3$  were predicted to be the same. It is a monoclinic  $P2_1/m$ -type structure that consists of zigzag chains of boron along the [100] direction [Fig. 1(a)]. As a result of strong covalent bonding, the chains of boron are interconnected to form a planar structure of closed six-member rings; this motif has been previously observed in  $ReB_2$  [14]. Notably, for  $Ir_2B_3$ , the predicted  $P2_1/m$  structure is found to have much lower energy, i.e., by  $\sim 1.02 \text{ eV/f.u.}$ , than the  $C2/m$  structure [35] previously proposed for the synthesized Ir-B compound (see Tables S3 and S4 in the Supplemental Material [46]). For the  $MB_2$  stoichiometry, the predicted ground state structures of  $CoB_2$ ,  $RhB_2$ , and  $IrB_2$  were different at ambient pressure. They are the hexagonal  $P6_3/mmc$  structure for  $CoB_2$ ,  $C2/m$  structure for  $RhB_2$ , and a different  $C2/m$  structure for  $IrB_2$  [Figs. 1(b)–1(d)]. All three predicted structures are calculated to be more stable than the previously proposed structures [34,47,48] (see Supplemental Material for structure parameters in Tables S1–

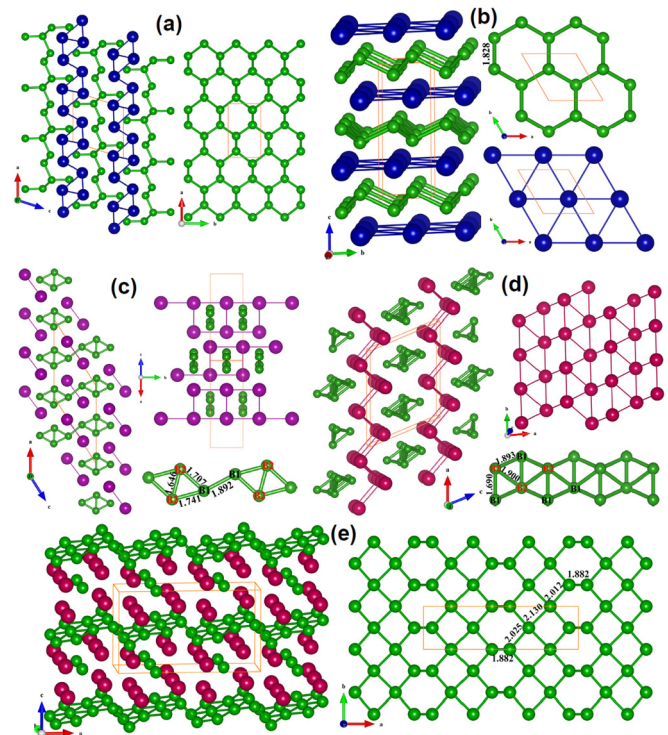


FIG. 1. (Color online) (a) Crystal structure of the  $P2_1/m$ -type  $M_2B_3$  ( $M = \text{Co, Rh, and Ir}$ ), which contains conjugated boron rings or double-connected zigzag boron chains with two nonequivalent boron sites (Wyckoff  $2e$ ). Crystal structures for (b)  $CoB_2$ , (c)  $RhB_2$ , (d)  $IrB_2$ , and (e)  $IrB_{1.25}$  ( $Ir_4B_5$ ) at ambient pressure. The shortest B-B distance in  $CoB_2$  is 1.828 Å. The neighboring  $B_4$  rhomboids in  $RhB_2$  are connected by a  $\sigma$  bond with a length of 1.892 Å. In the  $B_4$  rhomboid, the lengths of two edges are 1.707 and 1.741 Å, respectively, whereas the central bond is shorter, 1.646 Å. In  $IrB_2$ , the two edges of the butterflylike  $B_4$  units are 1.690 and 1.893 Å, respectively, whereas the central bond is 1.900 Å. The smallest value of B-B-B angles in  $B_4$  rhomboid is  $57.0^\circ$  in  $RhB_2$  and  $52.9^\circ$  in  $IrB_2$ . Green spheres represent B atoms; blue, purple, and red spheres represent metal atoms hereafter. Complete sets of lattice parameters and atomic coordinates are given in Tables S1–S3 and Tables S5–S7 of the Supplemental Material [46].

S3 [46]). In particular, the  $OsB_2$ -type [49] and  $C2/m$ -type [34] structures of  $IrB_2$  were found to be energetically unfavorable because of a large heat of formation (see Supplemental Material [46]).

The established phase stabilities of  $IrB_2$  and  $Ir_2B_3$  ( $IrB_{1.5}$ ) provided us critical guidance for resolving the structure of the first synthesized Ir-B compound [33]. At first, we examined all previously proposed structure models for this compound [33–35], including one  $IrB_2$  structure and six  $Ir_8B_{12}$  ( $IrB_{1.5}$ ) structures. Total energy calculations showed that the  $IrB_2$  structure is thermodynamically unstable with respect to the elemental solids, with a positive heat of formation  $\Delta H_f$  of 0.11 eV/atom (see Supplemental Material Table S4 [46]). Furthermore, the calculated x-ray diffraction (XRD) pattern of the  $IrB_2$  structure does not match the experimental results, which rules out this possibility. Two  $Ir_8B_{12}$  structures,  $Ir_8B_{12}$ -VI and  $Ir_8B_{12}$ -V (definitions adopted from Ref. [34] hereafter) were calculated to have negative heat of formation,  $-0.028$

and  $-0.157$  eV/atom, respectively (see Supplemental Material Table S4 [46]). However, the lattice parameters of these two structures are likely to differ from those of the experimental phase, as seen again from the insufficient matches of the XRD patterns (see Supplemental Material Table S4 and Fig. S1 [46]). A detailed analysis of these  $\text{Ir}_8\text{B}_{12}$  structures revealed useful information for the Ir-B system. The  $\text{Ir}_8\text{B}_{12}$  structures all have the same parent structure but differ in the site occupancies of the boron atoms. The total energy of an  $\text{Ir}_8\text{B}_{12}$  structure was found to be particularly sensitive to the occupancy of the two sites, B (VI) and B (V). A partial or complete removal of boron from these two sites, as in the cases of  $\text{Ir}_8\text{B}_{12}\text{-VI}$  and  $\text{Ir}_8\text{B}_{12}\text{-V}$ , seems to be a reason for their thermodynamic stabilities (as opposed to other  $\text{Ir}_8\text{B}_{12}$  structures with fully occupied VI and V sites).

As suggested, the synthesized Ir-B compound may have a lower boron concentration than  $\text{IrB}_{1.5}$  [34,35]. To examine this possibility, we carried out an exhaustive search for the stable  $\text{Ir}_8\text{B}_{11}$  ( $\text{IrB}_{1.375}$ ) and  $\text{Ir}_8\text{B}_{10}$  ( $\text{IrB}_{1.25}$ ) phases based on the known  $\text{Ir}_8\text{B}_{12}$  ( $\text{IrB}_{1.5}$ ) structures. Candidate  $\text{Ir}_8\text{B}_{11}$  and  $\text{Ir}_8\text{B}_{10}$  structures were constructed by removing a certain number of boron atoms from possible sites in the supercells of  $\text{Ir}_8\text{B}_{12}\text{-V}$  and  $\text{Ir}_8\text{B}_{12}\text{-VI}$  [34] (see Supplemental Material [46] for details of the method). The resulting structures were then fully relaxed to energy minima. The calculated energies of the relaxed structures confirmed that the structures with empty V or VI site tend to have lower energies (see Supplemental Material for Table S4 [46]). For the  $\text{Ir}_8\text{B}_{11}$  ( $\text{IrB}_{1.375}$ ) stoichiometry, two structures ( $P2/m$  and  $P2_1/m$ ) were calculated to have extraordinary low heat of formation, i.e.,  $-0.29$  and  $-0.27$  eV/atom (see Supplemental Material Table S4 [46]), but their XRD patterns differ largely from the experimental results (see Supplemental Material Fig. S1 [46]). On the other hand, the structure search on the  $\text{Ir}_8\text{B}_{10}$  ( $\text{IrB}_{1.25}$ ) stoichiometry (see Supplemental Material Table S4 [46]) revealed these findings: a  $Cm$  structure with similar heat of formation ( $-0.31$  eV/atom), and the lattice parameters appear to be consistent with the experiment. Significantly, in the  $Cm$  structure boron atoms are completely absent at the V sites and only occupy half of the VI sites, which is in agreement with the site preferences and also consistent with the experimental expectations [34]. As shown in Fig. 1(e), the  $Cm$  structure of  $\text{IrB}_{1.25}$  has an interesting sandwich structure with alternative layers of stepwise boron sheets and isolated B and Ir atoms. The boron sheets extend through the  $ab$  plane with relatively weaker interaction due to slightly longer B-B distances ( $1.882\text{--}2.130$  Å). Furthermore, the calculated XRD pattern of the  $Cm$  structure shows a remarkable good match to the experimental spectrum (Fig. 2). Both the peak positions and relative intensities of the calculated XRD pattern match perfectly with those of the experiment, suggesting the  $Cm$  phase is very likely to be the observed one. This prediction agrees with earlier structural refinements in which the  $Cm$  symmetry was considered as one of the possible space groups for the Ir-B compound, which was, however, never substantiated [35]. To this end, supported by both energetics and structure information, we suggest that the long-standing unidentified Ir-B compound has an  $\text{IrB}_{1.25}$  stoichiometry and a  $Cm$  structure, which hopefully can be confirmed in future experiments.

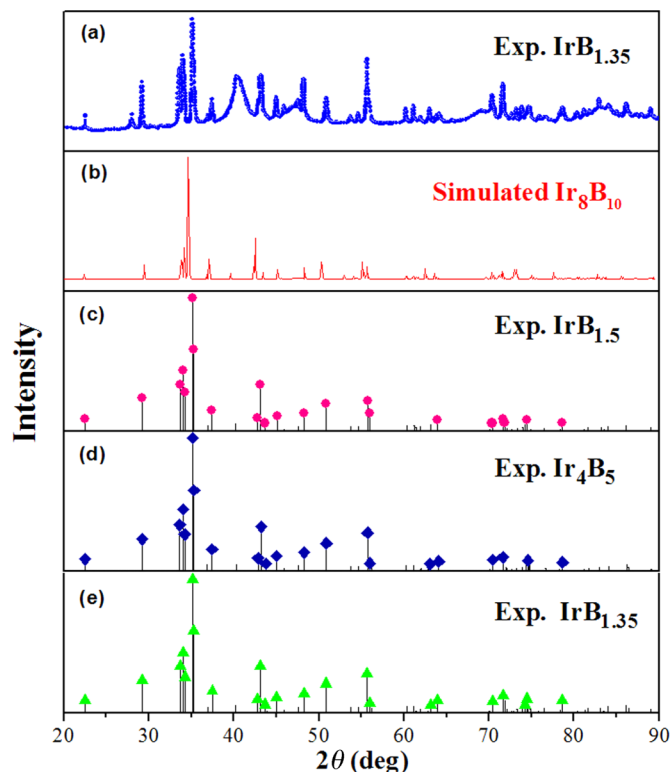


FIG. 2. (Color online) Simulated XRD pattern of the predicted  $\text{IrB}_{1.25}$  phase (b) compared to experimentally measured pattern along with the previous suggested stoichiometries. Experimental data in (a), (c), (d), and (e) were reported in Refs. [33–36], respectively. A wavelength of  $1.5406$  Å is used.

Moving to a higher boron concentration, the predicted ground state structures for  $\text{IrB}_3$ ,  $\text{RhB}_3$ , and  $\text{CoB}_3$  are again the same. This structure [Fig. 3(a)] has the  $Pnma$  space group and is isostructural to  $\text{RuB}_3$  [50]. In this structure, boron atoms form  $\text{B}_3$  scalene units through three-center two-electron ( $3c, 2e$ ) bonding. The scalene units are interconnected into a three dimensional network, whereas the zigzag chains of metal atoms intersperse along the  $[010]$  direction as electron donors. For the  $\text{MB}_{3.2}$  (or  $\text{M}_5\text{B}_{16}$ ) stoichiometry, the only thermodynamically stable structure found was  $\text{CoB}_{3.2}$ . Both the  $\text{IrB}_{3.2}$  and  $\text{RhB}_{3.2}$  structures were calculated to have large positive heat of formation (see Supplemental Material Tables S2 and S3 [46]). The  $\text{CoB}_{3.2}$  structure has been known experimentally [30], and the calculated structural parameters are in good agreement with the experimental data (see Supplemental Material Table S1 [46]). In the  $\text{CoB}_{3.2}$  structure, the boron atoms are clustered into two forms: localized  $\text{B}_3$  triangular units and extended  $\text{B}_\infty$  ribbons [Fig. 3(b)]. The buckled boron ribbon is a characteristic feature of superhard borides. Furthermore, the remarkably shorter Co-Co distances indicate the possible presence of metal-metal bonds in this structure.

The stoichiometry of the highest boron content investigated in the present paper is  $\text{MB}_4$  (tetraborides). Tetraborides have been realized previously in  $\text{CrB}_4$ ,  $\text{FeB}_4$ , and  $\text{MnB}_4$  [20–23], and are also possible for  $\text{MoB}_4$  [24] and  $\text{WB}_4$  [15,39,51]. Tetraborides containing main group elements, i.e.,

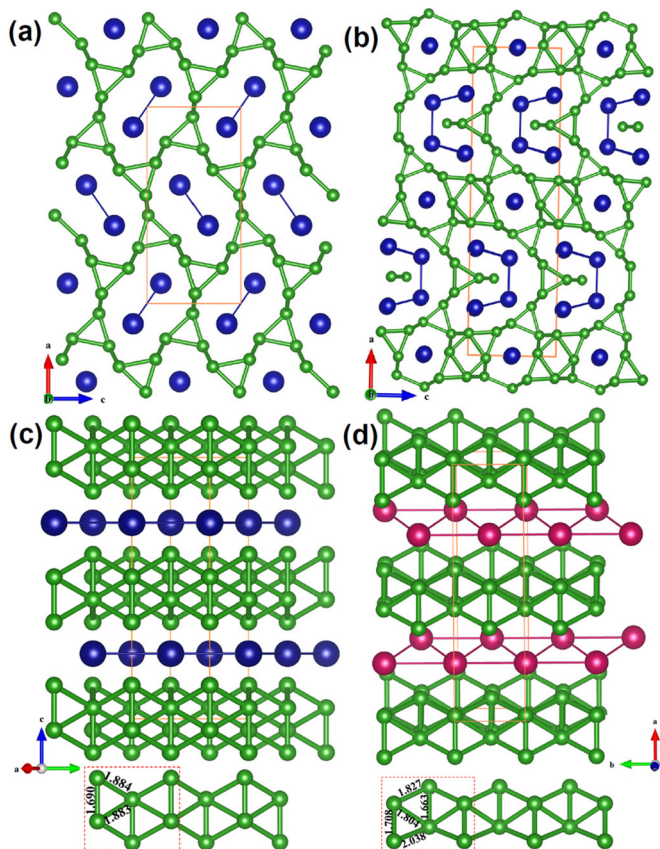


FIG. 3. (Color online) Crystal structures of (a)  $\text{CoB}_3$  and (b)  $\text{Co}_5\text{B}_{16}$ , both with distinct triangular  $\text{B}_3$  units. Crystal structures of  $h\text{-CoB}_4$  (c) and  $m\text{-IrB}_4$  (d). Bond lengths of the three B-B bonds in the  $\text{B}_4$  unit in  $h\text{-CoB}_4$  are 1.690, 1.884, and 1.883 Å. In  $m\text{-IrB}_4$ , the  $\text{B}_4$  unit is distorted with two short edges (1.663 and 1.708 Å), two long edges (1.831 and 2.034 Å), and the central bond (1.802 Å). Complete sets of lattice parameters and atomic coordinates are given in Tables S1–S3 and Tables S5–S7 of the Supplemental Material [46].

alkali metals, were also predicted to be thermodynamically stable under high pressure [52]. For  $\text{RhB}_4$  and  $\text{IrB}_4$ , an unprecedented monoclinic ( $m$ -)  $C2/m$ -type structure was found in our structural search as the common ground state structure [Fig. 3(d)]. We term this structure in  $\text{RhB}_4$  and  $\text{IrB}_4$  phases as  $m\text{-RhB}_4$  and  $m\text{-IrB}_4$ , respectively. The  $\text{CoB}_4$ , on the other hand, was predicted to have a hexagonal structure [termed as  $h\text{-CoB}_4$ , Fig. 3(c)], which is isotypical to  $\text{MoB}_4$  [24]. It is interesting that the  $\text{CoB}_4$  does not adopt the same orthorhombic structure of  $\text{FeB}_4$  [23]. Both  $m\text{-IrB}_4$  and  $h\text{-CoB}_4$  structures consist of alternating metal layers and puckered boron sheets, whereas the stacking pattern of these layers and sheets determines the space group.

Experimental synthesis of transition-metal borides often requires high-pressure high-temperature conditions. A fair share of the known transition-metal borides are only thermodynamically stable at high pressures but exhibit metastability at ambient conditions, which makes their recovery possible. To provide guidance for future experiments, we evaluated the pressure-composition phase diagrams for the Co-B, Rh-B, and Ir-B systems using the experimentally known and newly

predicted structures. The convex hull (decomposition tie line) is constructed at three different pressures for Co-B [Figs. 4(a) and 4(b)], Rh-B [see Supplemental Material Figs. S2(a) and S2(b) [46]], and Ir-B [Figs. 4(c)–4(e)] systems, respectively.

For the Co-B system, all considered cobalt borides are thermodynamically stable with respect to the Co and B solids at ambient pressure [Fig. 4(a)]. The calculated  $\Delta H_f$  of the cobalt-rich borides ( $\text{Co}_3\text{B}$ ,  $\text{Co}_2\text{B}$ , and  $\text{CoB}$ ) reproduces well the experimental energy orders [53] and identified the  $\text{CoB}$  as the most stable phase [2]. The  $\text{Co}_3\text{B}$  and  $\text{Co}_2\text{B}$  phases observed experimentally at high temperatures [54] were found to be metastable at ambient pressure, where their energies are slightly above the tie line. The newly predicted boron-rich phases also show metastability at ambient pressure. Their energies are very close to the tie line (e.g.,  $\text{Co}_5\text{B}_{16}$ ) and thus might be stabilized at finite temperatures by entropy effects. At high pressures, the  $\Delta H_f$  values of all Co-B stoichiometries decrease considerably relative to the enthalpies of the Co and B solids, whereas  $\text{CoB}$  remains as the most stable phase. In general, the  $\Delta H_f$  values of the boron-rich phases are very close to the tie line; therefore, the phase competition will be severe during synthesis, which may pose a challenge for phase separations in experiment [23]. Notably, the experimentally synthesized  $\text{Co}_5\text{B}_{16}$  phase becomes thermodynamically stable near 10 GPa, where its  $\Delta H_f$  value falls on the tie line [Fig. 4(a)]. When recalculated using the decomposition of  $\text{CoB}$  and boron solids, the  $\Delta H_f$  values of all Co-B stoichiometries become positive at ambient pressure [Fig. 4(b)]. The  $\text{Co}_5\text{B}_{16}$  phase again becomes thermodynamically stable near 10 GPa, where its  $\Delta H_f$  turns negative ( $\Delta H_f$  value is  $-0.14$  eV/f.u. at 20 GPa). The predicted threshold for the phase stability of  $\text{Co}_5\text{B}_{16}$  agrees very well with the pressure conditions used in the synthesis, i.e.,  $\sim 13\text{--}15$  GPa [30].

For the Ir-B system, the  $\text{IrB}_{1.25}$  phase predicted in the present paper is the most energetically favorable phase at ambient pressure with the lowest heat of formation [denoted as  $\text{Ir}_4\text{B}_5$  in Figs. 4(c)–4(e)]. This finding further validates the  $\text{IrB}_{1.25}$  as the experimentally realized Ir-B phase. All other predicted Ir-B phases stay above the tie line of convex hull, although they do have negative heats of formation. Upon increasing the pressure, the predicted monoclinic  $\text{IrB}_4$  phase moves on the tie line at 40 GPa, suggesting it may be synthesized under high-pressure conditions. Significantly, the realization of  $\text{IrB}_4$  phase becomes even more viable at pressures above 37 GPa (39 GPa), if the mixture of  $\text{Ir}_4\text{B}_5$  and B ( $\text{IrB}$  and B) powders are used [Figs. 4(d) and 4(e)]. In addition, the predicted orthorhombic  $Pnma$  structure of  $\text{IrB}_3$  may also be realized using the mixture of  $\text{Ir}_4\text{B}_5$  and boron at pressures above 70 GPa (not shown). For the Rh-B system, all Rh-rich phases are stable with respect to the Rh and B solids, where the Rh monoboride ( $\text{RhB}$ ) is the energetically most favorable phase [see Supplemental Material Fig. S2(a) [46]]. The B-rich phases, on the other hand, always stay above the tie line at ambient and high pressures (20 and 40 GPa). Furthermore, these phases are highly persistent even by the reaction of mixture of  $\text{RhB}$  and boron powders under pressure [see Supplemental Material Fig. S2(b) [46]], suggesting that alternative reaction routes are required for their synthesis.

Electronic and bonding properties of the predicted phases were analyzed to further reveal the structural features and

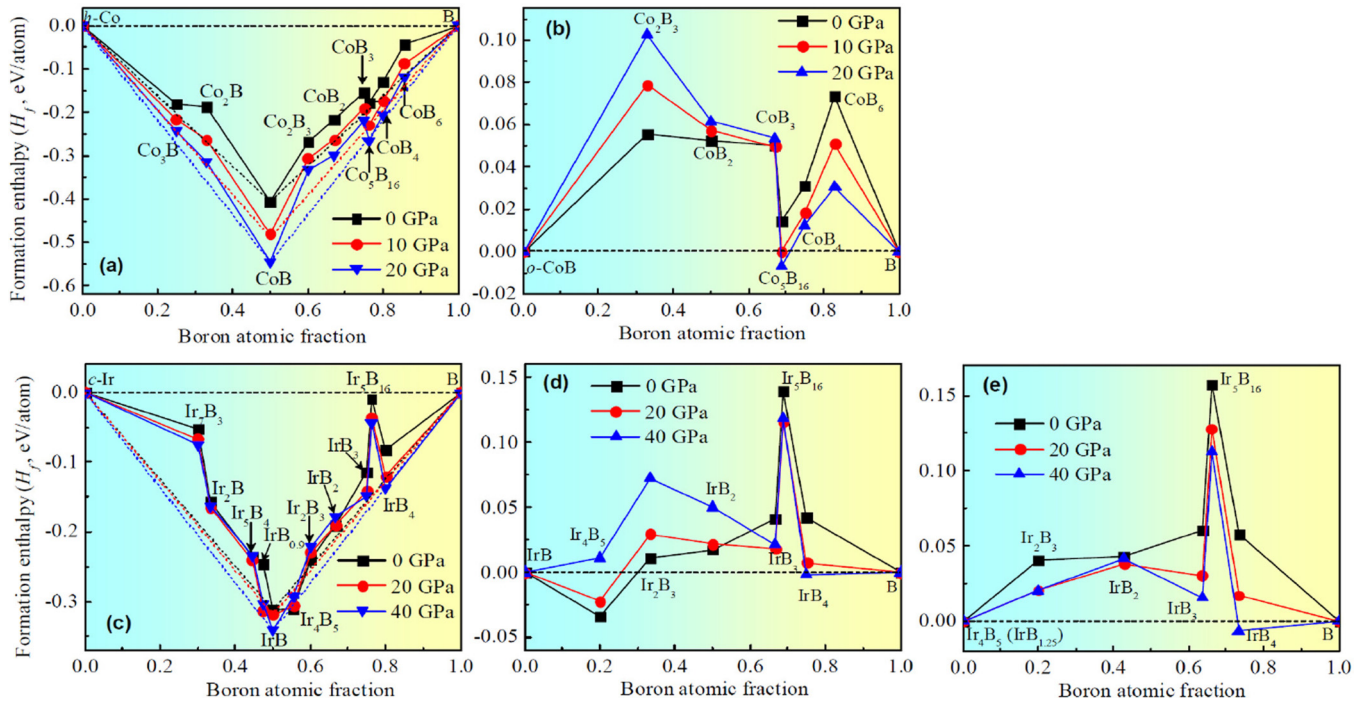


FIG. 4. (Color online) Calculated pressure-composition phase diagrams for the Co-B and Ir-B systems. Heat of formation of the  $\text{CoB}_x$  phases at ambient and high pressures relative to (a) elemental Co and B solids and to (b) CoB and B solids. The FeB-type structure has been used for CoB. Heat of formation of the  $\text{IrB}_x$  phases at ambient and high pressures relative to (c) elemental Ir and B solids, to (d) IrB and B solids, and to (e)  $\text{Ir}_4\text{B}_5$  (this paper) and B solids. The IrB adopts the WC-type structure at 0 GPa and the anti-NiAs-type structure at 20 and 40 GPa. In all calculations, the structures of solid B are  $\alpha$ -B (0 GPa), and  $\gamma$ -B (20 and 40 GPa).

elastic and mechanical performances. Most of the proposed group 9 metal borides are predicted to be metallic in view of the calculated density of states (DOS; see Supplemental Material Figs. S9–S11 [46]). Note that some of the predicted borides were found to have a tunable band gap subject to elastic strains. One example is given in Fig. S12 (see Supplemental Material [46]), in which the orthorhombic  $Pnma$ -type  $\text{IrB}_3$ , otherwise being weakly metallic, opens up an indirect band gap of about 0.25 eV under 5% tensile strength. In the following, we present a detailed analysis of electronic structure and bonding features of  $\text{Co}_5\text{B}_{16}$  and  $\text{IrB}_4$ . The calculated total, site-projected, and orbital-projected DOS of orthorhombic  $\text{CoB}_3$  and  $\text{Co}_5\text{B}_{16}$  phases are presented and compared in Figs. 5(a)–5(c). Clearly, the  $3d$  states of Co contribute significantly to the valence bands (VB) of both borides. The Fermi level falls into a pseudogap for  $\text{Co}_5\text{B}_{16}$  and the edge of antibonding region of Co- $3d$  states for  $\text{CoB}_3$ , respectively. Both structures feature a strong hybridization between the  $2p$  states of boron and  $3d$  states of cobalt throughout the valence region, in particular, between  $-10$  to  $-2$  eV. Figure 5(c) shows the orbital-projected DOS of  $\text{Co}_5\text{B}_{16}$ , in which the projection has been made to each individual  $p$  orbital of B atoms and to each  $d$  orbital of the Co atoms. The B atoms in the three triangular planers are noted by  $\text{B}_3$ -1,  $\text{B}_3$ -2,  $\text{B}_3$ -3. As expected from the directional interactions, the three  $p$  orbitals contribute quite differently to the DOS in the three triangles. In the  $\text{B}_3$ -1 triangle, they contribute almost equally, while in  $\text{B}_3$ -2 and  $\text{B}_3$ -3 triangles, some orbitals make more contributions than others. The  $d_{xy}$  and  $d_{xz}$  orbitals of the Co-2 and Co-3 atoms have significant

contributions to the covalent hybridizations of B and Co atoms, whereas the  $d_{x^2-y^2}$  orbital of all the Co atoms are located close to the Fermi level.

The bonding environment of  $\text{Co}_5\text{B}_{16}$  was investigated using the electron localized function (ELF) method. As an intuitive approach, the ELF method characterizes the tendency of electron localization in crystals, with respect to a uniform electron gas of the same density. As it is a probability, the ELF value is always positive and spans the range between 0 and 1. Large ELF values identify regions in the structure where there is a high tendency of electron pairing, such as cores, bonds, and lone pairs. In Fig. 5(d), the ELF isosurface is shown for the  $\text{Co}_5\text{B}_{16}$  structure, which reveals neatly its bonding pattern. Electrons clearly tend to pair in the centers of the three triangles. The corresponding ELF values in the center of the three triangles are 0.83 ( $\text{B}_3$ -1), 0.84 ( $\text{B}_3$ -2), and 0.85 ( $\text{B}_3$ -3), respectively. Large ELF values in the voids indicate the presence of secondary attractive interactions that stabilize the triangles. The high tendency of electron localizations is also identified in the intertriangle regions along the zigzag boron strand (ELF: 0.85) that are associated with the  $\sigma$  bonds. Long pairs are identified in spaces slightly outside the edge-shared buckled hexagonal boron rings (ELF: 0.88). As such, the entire boron framework is stabilized by the electrons transferred from the Co atoms, as explained by the Zintl concept. The amounts of charge transfer as inferred from the DOS are  $+1.5e$  for a Co-3 atom,  $+1.2e$  for a Co-2 atom, and  $+1.1e$  for a Co-1 atom, respectively. Negatively charged boron triangles effectively shield the repulsive interactions

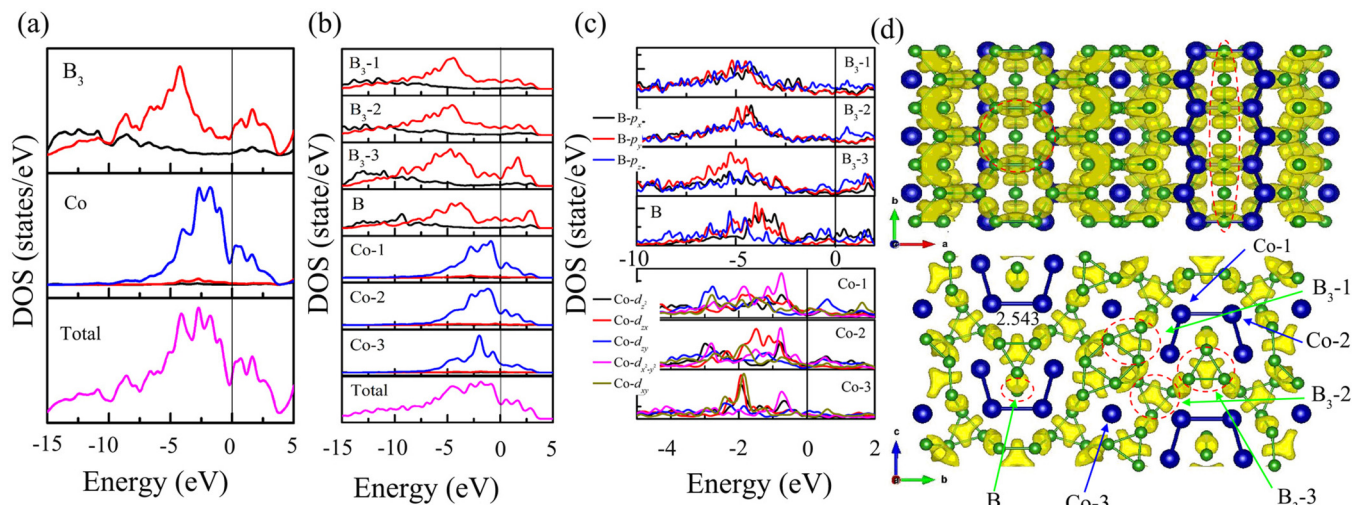


FIG. 5. (Color online) Calculated DOS of (a) CoB<sub>3</sub> and (b) Co<sub>5</sub>B<sub>16</sub>. Black, red, and blue curves represent the projected DOS to *s*, *p*, and *d* orbitals, respectively, while the pink curve represents the total DOS. (c) Projected DOS to individual *p* orbitals of B and to individual *d* orbitals of Co in Co<sub>5</sub>B<sub>16</sub>. (d) Calculated electron localization function of Co<sub>5</sub>B<sub>16</sub>.

between Co cations in Co<sub>5</sub>B<sub>16</sub>, which results in short Co-Co distances.

The calculated total and atom-projected DOS of RhB<sub>4</sub> and IrB<sub>4</sub> are shown in Fig. 6(a). Both structures are metallic, as observed from the absence of the band gaps. In RhB<sub>4</sub>, the Fermi level falls in a local energy minimum. Thus, the DOS value at the Fermi level is very low. In the IrB<sub>4</sub>, a pseudogap tends to open near the Fermi level, yielding an

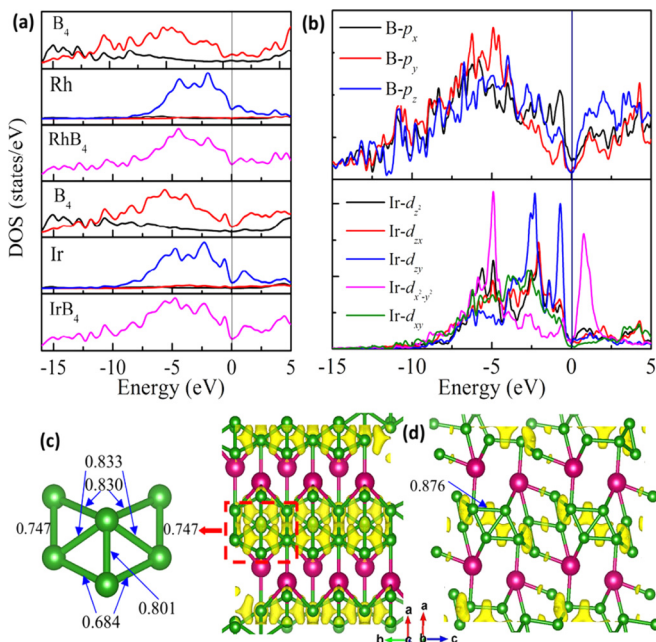


FIG. 6. (Color online) (a) Calculated DOS of RhB<sub>4</sub> and IrB<sub>4</sub>. Black, red, blue, and pink curves represent *s*-, *p*-, and *d*-projected DOS and total DOS, respectively. (b) Projected DOS to individual *p* orbitals of B and to individual *d* orbitals of Ir in IrB<sub>4</sub>. (c) Calculated MOP value in typical butterflylike B<sub>4</sub> units in IrB<sub>4</sub>. (d) Calculated electron localization function of IrB<sub>4</sub>.

even lower DOS, while stabilizing the structure. Moreover, the hybridization between the *d* orbitals of Ir and *p* orbitals of B is relatively strong at the energy of -10 eV to the Fermi level due to the spatial diffusion of 5*d* orbitals. Figure 6(b) shows the contributions of individual orbitals of B<sub>4</sub> unit and Ir atoms to the DOS. The *p<sub>x</sub>* orbital of the B<sub>4</sub> is seen to contribute more than *p<sub>y</sub>* and *p<sub>z</sub>* to the DOS at the Fermi level. There is also a distinct splitting between the bonding and antibonding regions for the *d<sub>x<sup>2</sup>-y<sup>2</sup></sub>* bands of Ir. The bands by antibonding orbitals are primarily localized within ~1 eV above the Fermi level. The orbital overlaps stabilize the bonding interactions and destabilize the antibonding interactions and therefore stabilize the IrB<sub>4</sub> structure. As a result, the total energy is lowered, and a pseudogap tends to open at the Fermi level. The calculated ELF for IrB<sub>4</sub> is presented in Fig. 6(c), which clearly reveals the presence of strong covalent  $\sigma$  bonds and distorted electron-deficient B-B-B (3c, 2e) bonding. In the butterfly-B<sub>4</sub> units, the bonding electrons are localized in the center of triangular planes caused by an asymmetrical arrangement of the boron bonds. The central B-B bond in the B<sub>4</sub> units has a relatively large ELF value, 0.833, while the long edge has a lower value, 0.684, both within the covalent region. The maximum ELF value for the B-B bonds is 0.876 [Fig. 6(d)], which interconnects butterfly-B<sub>4</sub> units along the [001] direction. The high tendency of electron localization is also observed between Ir and B atoms, with the ELF values ranging from 0.697 to 0.806. The spatial orientations of covalent bonding, therefore, play a critical role in the energetic stability of this compound.

#### IV. CONCLUSIONS

In summary, extensive theoretical searches for stable compositions and crystal structures of group 9 borides (*MB<sub>x</sub>*, *M* = Co, Rh, and Ir, *x* = 1.5, 2, 3, 4, and 6) were carried out using an unbiased structure searching method within the CALYPSO code. We have predicted a series of new *MB<sub>x</sub>*

stoichiometries, stable at ambient or high pressures or both and explored the possible synthetic pathways. Significantly, we have successfully addressed the long-sought composition and structure of the first synthesized Ir-B compound. We propose this compound to have a novel IrB<sub>1.25</sub> stoichiometry and a monoclinic *Cm* structure. The *Cm* structure is thermodynamically stable, and its interplanar spacings correspond very well to the measured diffraction patterns. Predicted borides of different stoichiometries exhibit a variety of boron networks, ranging from zigzag chains in *M*<sub>2</sub>B<sub>3</sub>, regular rhomboids in *MB*<sub>2</sub>, triangles in *MB*<sub>3</sub> and *MB*<sub>3,2</sub>, to distorted rhomboids in *MB*<sub>4</sub>. The results obtained in the present paper will hopefully provide insight and guidance to future experimental investigations of transition-metal borides.

## ACKNOWLEDGMENTS

We thank Dr. S. V. Ovsyannikov, Prof. X.-j. Chen, and Dr. I. Naumov for critically reading the paper. This work was supported by National Natural Science Foundation of China under Grants No. 51201148 and No. U1530402, and by Natural Sciences and Engineering Research Council of Canada through a Discovery grant. L.W. thanks the foundation of Hebei Province Education Department under Grant No. QN2014114 and the Autonomic Research Project of Yanshan University under Grant No. 13LGB007. Z.L. thanks Hebei Natural Science Foundation (Grant No. B2015203096) and the Autonomic Research Project of Yanshan University under Grant No. 14LGA017. Y.W. and L.W. contributed equally to this paper.

- 
- [1] B. Albert and H. Hillebrecht, *Angew. Chem., Int. Ed.* **48**, 8640 (2009).
- [2] A. G. Van der Geest and A. N. Kolmogorov, *Calphad* **46**, 184 (2014).
- [3] Y. Yao and R. Hoffmann, *J. Am. Chem. Soc.* **133**, 21002 (2011).
- [4] R. B. Kaner, J. J. Gilman, and S. H. Tolbert, *Science* **308**, 1268 (2005).
- [5] A. P. Sergeeva, I. A. Popov, Z. A. Piazza, W.-L. Li, C. Romanescu, L.-S. Wang, and A. I. Boldyrev, *Acc. Chem. Res.* **47**, 1349 (2014).
- [6] Q. Gu, G. Krauss, and W. Steurer, *Adv. Mater.* **20**, 3620 (2008).
- [7] T. Ogitsu, F. Gygi, J. Reed, Y. Motome, E. Schwegler, and G. Galli, *J. Am. Chem. Soc.* **131**, 1903 (2009).
- [8] J. B. Levine, S. H. Tolbert, and R. B. Kaner, *Adv. Funct. Mater.* **19**, 3519 (2009).
- [9] M. M. Balakrishnarajan and R. Hoffmann, *J. Am. Chem. Soc.* **126**, 13119 (2004).
- [10] A. N. Kolmogorov and S. Curtarolo, *Phys. Rev. B* **74**, 224507 (2006).
- [11] A. L. Ivanovskii, *Prog. Mater. Sci.* **57**, 184 (2012).
- [12] J. Kortus, I. I. Mazin, K. D. Belashchenko, V. P. Antropov, and L. L. Boyer, *Phys. Rev. Lett.* **86**, 4656 (2001).
- [13] R. Lortz, Y. Wang, U. Tutsch, S. Abe, C. Meingast, P. Popovich, W. Knafo, N. Shitsevalova, Yu. B. Paderno, and A. Junod, *Phys. Rev. B* **73**, 024512 (2006).
- [14] H.-Y. Chung, M. B. Weinberger, J. B. Levine, A. Kavner, J.-M. Yang, S. H. Tolbert, and R. B. Kaner, *Science* **316**, 436 (2007).
- [15] R. Mohammadi, A. T. Lech, M. Xie, B. E. Weaver, M. T. Yeung, S. H. Tolbert, and R. B. Kaner, *Proc. Natl. Acad. Sci. USA* **108**, 10958 (2011).
- [16] X. Zhang, N. P. Butch, P. Syers, S. Ziemak, R. L. Greene, and J. Paglione, *Phys. Rev. X* **3**, 011011 (2013).
- [17] G. Li, Z. Xiang, F. Yu, T. Asaba, B. Lawson, P. Cai, C. Tinsman, A. Berkley, S. Wolgast, Y. S. Eo, D.-J. Kim, C. Kurdak, J. W. Allen, K. Sun, X. H. Chen, Y. Y. Wang, Z. Fisk, and L. Li, *Science* **346**, 1208 (2014).
- [18] M. Neupane, N. Alidoust, S. Y. Xu, T. Kondo, Y. Ishida, D. J. Kim, C. Liu, I. Belopolski, Y. J. Jo, T. R. Chang, H. T. Jeng, T. Durakiewicz, L. Balicas, H. Lin, A. Bansil, S. Shin, Z. Fisk, and M. Z. Hasan, *Nat. Commun.* **4**, 2991 (2013).
- [19] N. Xu, P. K. Biswas, J. H. Dil, R. S. Dhaka, G. Landolt, S. Muff, C. E. Matt, X. Shi, N. C. Plumb, M. Radović, E. Pomjakushina, K. Conder, A. Amato, S. V. Borisenko, R. Yu, H.-M. Weng, Z. Fang, X. Dai, J. Mesot, H. Ding, and M. Shi, *Nat. Commun.* **5**, 4566 (2014).
- [20] H. Niu, J. Wang, X.-Q. Chen, D. Li, Y. Li, P. Lazar, R. Podloucky, and A. N. Kolmogorov, *Phys. Rev. B* **85**, 144116 (2012).
- [21] H. Gou, A. A. Tsirlin, E. Bykova, A. M. Abakumov, G. Van Tendeloo, A. Richter, S. V. Ovsyannikov, A. V. Kurnosov, D. M. Trots, Z. Konopkova, H.-P. Liermann, L. Dubrovinsky, and N. Dubrovinskaia, *Phys. Rev. B* **89**, 064108 (2014).
- [22] A. Knappschneider, C. Litterscheid, N. C. George, J. Brgoch, N. Wagner, J. Beck, J. A. Kurzman, R. Seshadri, and B. Albert, *Angew. Chem., Int. Ed.* **53**, 1684 (2014).
- [23] H. Gou, N. Dubrovinskaia, E. Bykova, A. A. Tsirlin, D. Kasinathan, W. Schnelle, A. Richter, M. Merlini, M. Hanfland, A. M. Abakumov, D. Batuk, G. Van Tendeloo, Y. Nakajima, A. N. Kolmogorov, and L. Dubrovinsky, *Phys. Rev. Lett.* **111**, 157002 (2013).
- [24] M. G. Zhang, H. Wang, H. B. Wang, T. Cui, and Y. M. Ma, *J. Phys. Chem. C* **114**, 6722 (2010).
- [25] M. Wang, Y. Li, T. Cui, Y. Ma, and G. Zou, *Appl. Phys. Lett.* **93**, 101905 (2008).
- [26] A. T. Lech, C. L. Turner, R. Mohammadi, S. H. Tolbert, and R. B. Kaner, *Proc. Natl. Acad. Sci. USA* **112**, 3223 (2015).
- [27] P. Salamakha, O. Sologub, C. Rizzoli, A. P. Gonçalves, and M. Almeida, *J. Solid State Chem.* **177**, 4237 (2004).
- [28] B. Aronsson, E. Stenberg, and J. Åselius, *Acta Chem. Scand.* **14**, 733 (1960).
- [29] R. W. Mooney and A. J. E. Welch, *Acta Crystallogr.* **7**, 49 (1954).
- [30] E. Bykova, A. A. Tsirlin, H. Gou, L. Dubrovinsky, and N. Dubrovinskaia, *J. Alloys Compd.* **608**, 69 (2014).
- [31] Y. Wang, L. Li, Y. Wang, D. Song, G. Liu, Y. Han, L. Jiao, and H. Yuan, *J. Power Sources* **196**, 5731 (2011).
- [32] B. I. Nörling, L.-E. Tergenius, and I. Westman, *J. Less-Common Met.* **82**, 303 (1981).
- [33] B. Aronsson, E. Stenberg, and J. Åselius, *Nature (London)* **195**, 377 (1962).
- [34] B. Aronsson, *Acta Chem. Scand.* **17**, 2036 (1963).
- [35] T. Lundstrom and L.-E. Tergenius, *Acta Chem. Scand.* **27**, 3705 (1973).
- [36] J. V. Rau and A. Latini, *Chem. Mater.* **21**, 1407 (2009).
- [37] Y. Wang, J. Lv, L. Zhu, and Y. Ma, *Phys. Rev. B* **82**, 094116 (2010).

- [38] Y. Wang, J. Lv, L. Zhu, and Y. Ma, *Comput. Phys. Commun.* **183**, 2063 (2012).
- [39] Q. Li, D. Zhou, W. Zheng, Y. Ma, and C. Chen, *Phys. Rev. Lett.* **110**, 136403 (2013).
- [40] F. Peng, M. Miao, H. Wang, Q. Li, and Y. Ma, *J. Am. Chem. Soc.* **134**, 18599 (2012).
- [41] M. D. Segall, P. J. D. Lindan, M. J. Probert, C. J. Pickard, P. J. Hasnip, S. J. Clark, and M. C. Payne, *J. Phys.: Condens. Matter* **14**, 2717 (2002).
- [42] J. P. Perdew, K. Burke, and M. Ernzerhof, *Phys. Rev. Lett.* **77**, 3865 (1996).
- [43] H. J. Monkhorst and J. D. Pack, *Phys. Rev. B* **13**, 5188 (1976).
- [44] A. Togo, F. Oba and I. Tanaka, *Phys. Rev. B* **78**, 134106 (2008).
- [45] A. R. Oganov *et al.*, *Nature (London)* **457**, 863 (2009).
- [46] See Supplemental Material at <http://link.aps.org/supplemental/10.1103/PhysRevB.92.174106> for computational methods and details, computed structural parameters, enthalpies of formation, structure stabilities, band structures, and DOS for Co, Rh, and Ir borides, simulated XRD patterns for IrB<sub>x</sub> compared with the experimental data, and energy selections for IrB<sub>1+x</sub> ( $0 < x < 0.5$ ).
- [47] W. J. Zhao and Y. X. Wang, *J. Solid State Chem.* **182**, 2880 (2009).
- [48] D. Y. Wang, B. Wang, and Y. X. Wang, *J. Phys. Chem. C* **116**, 21961 (2012).
- [49] H. Y. Gou, L. Hou, J. W. Zhang, H. Li, G. F. Sun, and F. M. Gao, *Appl. Phys. Lett.* **88**, 221904 (2006).
- [50] Y. Wang, T. Yao, L.-M. Wang, J. Yao, H. Li, J. Zhang, and H. Gou, *Dalton Trans.* **42**, 7041 (2013).
- [51] J. V. Rau, A. Latini, R. Teghil, A. De Bonis, M. Fosca, R. Caminiti, and V. R. Albertini, *Appl. Mater. Interfaces* **3**, 3738 (2011).
- [52] A. Hermann, A. McSorley, N. W. Ashcroft, and R. Hoffmann, *J. Am. Chem. Soc.* **134**, 18606 (2012).
- [53] G. L. W. Hart, S. Curtarolo, T. B. Massalski, and O. Levy, *Phys. Rev. X* **3**, 041035 (2013).
- [54] Y. Du, J. C. Schuster, Y. A. Chang, Z. Jin, and B. Huang, *Z. Metallk.* **93**, 1157 (2002).